

ASSESSING INTRA-BAR VARIATIONS IN GRAIN ROUGHNESS USING CLOSE-RANGE PHOTOGRAMMETRY

JANE GROOM, STÉPHANE BERTIN, AND HEIDE FRIEDRICH
Department of Civil and Environmental Engineering, University of Auckland, New Zealand
e-mail: jgro800@aucklanduni.ac.nz

ABSTRACT: Evidence of downstream fining in sediment size along the length of a gravel bar has frequently been observed. However, there is limited quantitative information on the variation of other roughness statistics. Developments in the acquisition of high-resolution topographic data provide the opportunity for assessing roughness variations along and across a gravel bar, to quantify existing theoretical observations of bar sorting. Here, close-range photogrammetry is used for the first time to assess intra-bar variations in roughness at 14 locations on a single gravel bar in the Whakatiwai River, New Zealand. An extensive range of roughness parameters are used, including the standard deviation of elevations, skewness, inclination index, and horizontal roughness lengths from second-order structure functions. A reduction with distance down bar was found in all roughness parameters, except skewness, along with a decrease in the variability of the data at the bar tail for all parameters. Lateral variation in roughness parameters was also assessed, showing evidence of an increase in roughness parameters with distance from the water edge. These findings can be used to validate and calibrate existing flow-resistance equations and morphodynamic models. General trends in roughness statistics indicate coarser sediment at the bar head and near the river bank. These trends reflect the formative flows and are used to infer sedimentation patterns, which suggest that the gravel bar undergoes development through lateral accretion. Although complexities in the sedimentation patterns are evident, due to multiple cycles of erosion and deposition, a greater understanding of these patterns is needed for the implementation of successful river management for this river, and others.

INTRODUCTION

Fluvial systems demonstrate reach-scale patterns in sedimentation, including downstream fining (i.e., a reduction in grain size) (Sternberg 1875). Although there is less published research on intra-bar variability, variations in sediment characteristics (e.g., size, sorting, and packing) across gravel bars contribute to bar morphology and, in turn, channel morphology (Ashworth and Ferguson 1986; Hardy 2006; Rice and Church 2010). The formation of bars occurs from spatial variations in sedimentation, including, but not limited to, lateral accretion and sediment accumulation due to flow convergence, which can result in down-bar fining of sediment (Leopold and Wolman 1957; Bluck 1976; Nanson 1980; Bluck 1982; Leopold 1992; Ashworth 1996; Burge 2006; Parker 2008). Due to feedbacks between channel morphology, sedimentation, and flow properties, the presence of gravel bars can alter flow properties and roughness at different scales, including reach, bar, and grain scale (Church and Jones 1982; Ashworth 1996; Church 2006; Raven et al. 2009; Bertoldi et al. 2009).

Roughness, resulting from these sedimentation patterns, is an important aspect in a fluvial system due to its influence on flow properties (including velocity and turbulence), sediment transport, and local ecology (Aberle and Nikora 2006; Hodge et al. 2009a; Baewert et al. 2014; Curran and Waters 2014). Estimations of roughness are important inputs for hydraulic and morphological models, along with models to determine the flow resistance in a channel (Aberle and Smart 2003; Tuijnder and Ribberink 2012).

Flow resistance results from forces that act on, and within, a flow to resist motion (Powell 2014), with various sources of energy loss in alluvial rivers. To calculate the flow's energy loss, hydraulic parameters such as velocity, depth, slope, and boundary shear stress must be predicted or calculated. Generally, there are three flow-resistance equations that are used in fluvial research: Darcy-Weisbach, Chezy, and Manning equations, of which all use roughness coefficients. The determination of these roughness coefficients is crucial for the calculation of flow resistance. However, determining the values of the coefficients is fraught with subjectivity, and thus they are often the main source of error in estimates of discharge and flow resistance (Powell 2014). Choosing the correct equation in flow modeling can be problematic, as an increasing number of modeling software programs calculate flow resistance automatically, without clarifying how it is calculated (Powell 2014). For example, flow modeling packages still use Manning's n as a roughness coefficient, although it has been identified as having many flaws, and there have been calls to move to a more robust alternative roughness coefficient (e.g., quantitative roughness parameters such as the standard deviation of elevations) (Ferguson 2010; Powell 2014).

Roughness is a term that is frequently used in literature, but it is rarely explicitly defined, which causes confusion (Smith 2014). Roughness is often used as a synonym for flow resistance, which suggests that roughness is a property of the flow rather than of a surface. Instead, we define grain roughness throughout this manuscript as the microtopography of the surface, resulting from the topography of individual grains; therefore

roughness is a property of the surface, with a pronounced effect on flow resistance.

Our understanding of bed roughness (i.e., microtopography of the surface) is facilitated by the development of technologies for the acquisition of high-resolution data. This includes (i) aerial photosieving (Carbonneau et al. 2004), which, although it can cover a large spatial scale, has been found to overestimate grain size; (ii) laser scanning (Milan et al. 2007; Entwistle and Fuller 2009; Heritage and Milan 2009; Brasington et al. 2012), which is expensive and time consuming; and (iii) structure-from-motion on unmanned aerial systems, which enables for the spatial variability of roughness to be assessed and inputted into morphodynamic models, although noise from reconstructions of up to 10 mm and blurry images are problematic (Vazquez-Tarrio et al. 2017). The technique of close-range photogrammetry (Bertin and Friedrich 2016) uses consumer-grade cameras (i.e., inexpensive), which can provide millimeter accuracy to address these aforementioned issues.

An increase in availability of large topographic datasets from these methods has led to an expansion in the literature of information about the grain size of the surface, which is used for calculating bed shear stress and estimating sediment transport (Pearson et al. 2017). Further, these large topographic datasets have resulted in the improved quantification of grain-roughness parameters. This includes bed-elevation moments from digital elevation models (DEMs), such as standard deviation of elevations, skewness, and kurtosis. These improvements signal a shift away from the previous use of roughness coefficients, percentiles of grain size, or roughness heights calibrated from flow measurements (Wilcock 1996; Smart et al. 2004; Aberle and Nikora 2006).

The aim of this paper is to obtain an improved understanding of bar-scale variations in grain-roughness parameters. There is little information regarding the grain-scale variations of surface structure and roughness in gravel surfaces (Bertin and Friedrich 2016). This is despite knowing that these aspects are key influences on flow resistance, sediment transport, and ecohydraulics (Aberle and Nikora 2006; Baewert et al. 2014; Curran and Waters 2014). This paper has three objectives:

1. To assess grain-roughness variability across the gravel bar, using an extensive range of roughness parameters; although bar-scale sorting is well documented (Rice and Church 2010), there is little quantification of this observation. Further, surface roughness of bars is rarely uniformly distributed, and its heterogeneity is of great interest (Smith 2014).
2. To examine roughness parameters and grain-size relationships, as research has investigated the relationship between grain size and the standard deviation of elevations (a common proxy for grain size). The influence of multiple factors including survey error, bed composition (e.g., packing, particle shape, sorting), and scale of roughness has been explored (Pearson et al. 2017), but further work is needed to understand and quantify these factors.
3. To understand if empirical roughness parameterization can lead to inferences concerning sedimentation patterns, which can provide insights into the physical processes that influence surface morphology (Hodge et al. 2009a).

METHODOLOGY

Data Collection

Data were obtained from the Whakatiwai River, a small gravel-bed stream in the Whakatiwai catchment (~ 1675 ha), which is located in northeast North Island, New Zealand (Fig. 1).

The stream has limited protection or management schemes (Hauraki District Council 2011), apart from stopbanks (levees) upstream and downstream of the gravel bar studied in this investigation. Previously,

cyclone Wilma (January 28–29, 2011) resulted in the stream undergoing significant lateral erosion in the stopbanked reaches, with calls from the community for management practices to be put in place. Surrounding areas of the stream mouth have high significance to the local iwi (Māori people), with urupā (burial ground) and wāhi tapu (sacred spiritual areas), and thus the local community is concerned with their protection. Recent channel-protection works include the insertion of gabion baskets, although these are thought to be of limited effect due to channel movement (Hauraki District Council 2011).

Our field observations at the time of data collection include bank erosion and evidence of animal activity on exposed gravel bars upstream of the study site, due to the surrounding farmland. This study focuses on an exposed gravel bar, located 300 meters upstream from the stream mouth. This gravel bar was chosen due to ease of accessibility with equipment from the road, and because previous field investigations using close-range photogrammetry were also undertaken at this site (Bertin and Friedrich 2016). Upstream areas of the bar were vegetated with clusters of dense pampas grass, and there was a change in elevation towards the water edge, with a slope vegetated by grass. The gravel bar selected for this investigation did not display signs of animal activity or disturbance and was opposite a rock revetment structure (Figs. 1C, 2A, B). The bar is not surrounded by accessible farmland, but instead is attached to a densely vegetated bank (Fig. 2). Google Earth images provide an indication to the evolution of this gravel bar over time, with the apparent propagation of the bar downstream (Fig. 2).

A 30-meter tape measure was placed along the bar, and care was taken to walk along this transect in order to not destroy natural sedimentation patterns, and measurement locations were placed either side of the transect, on non-disturbed areas. Measurement locations (Fig. 3), termed patches herein, were partially systematically chosen, covering down-bar and lateral patterns, although they were not evenly spaced (due to the deliberate attempt to avoid vegetated areas). Distances between patches were measured with a tape measure in the field, and later verified using a scaled orthophoto of the bar (Fig. 3). The orthophoto of the bar was taken using GoPro cameras at a height of 2 meters above the gravel surface. Subsequently, for analysis, the gravel bar was split into three sections every 10 meters down the bar, differentiating between bar-head, bar-center, and bar-tail regions (Fig. 3), similar to the method used by Rice and Church (2010) who evaluated grain-size variability by choosing sites that were representative of dominant textural facies.

At each patch, surface structure and grain size were measured using close-range digital photogrammetry (Fig. 1). Here, two Nikon D5100 cameras with Nikkor 20 mm lenses in tandem (16.4 Mpixel, 23.6 mm × 15.6 mm sensor size), were used to take photos of the gravel surface. The cameras were calibrated in the laboratory before accessing the field (see section on analytical methods). Then the camera rig (horizontal metal frame) was kept in a wooden transportation box in order to reduce any movement in the camera setup during travel to the field. This has been found to have minimal disturbance to the (pre-calibrated) cameras and provide adequate results for high-quality DEMs with vertical accuracies, determined with a 3D-printed gravel bed and represented by the mean unsigned error between measurements and true values, of less than 1 mm (Bertin and Friedrich 2016). Once in the field, the camera rig was gently put on top of two tripods, placed ~ 1 m apart, and screwed securely in place. The cameras were at an approximate height of 75 cm from the gravel surface, as determined from a setup selection in the laboratory. Finally, two laptops were attached by cables to each camera, in order to remotely capture the photographs of the surface. Further details into the field use of close-range photogrammetry are found in Bertin and Friedrich (2016).

A repeat calibration was completed in the field, as transporting the stereo setup is critical, and this provided the opportunity to determine the suitability of field calibration. Evaluation of the maximum field rectification error provided lower values of 0.47 pixel, compared to 0.88

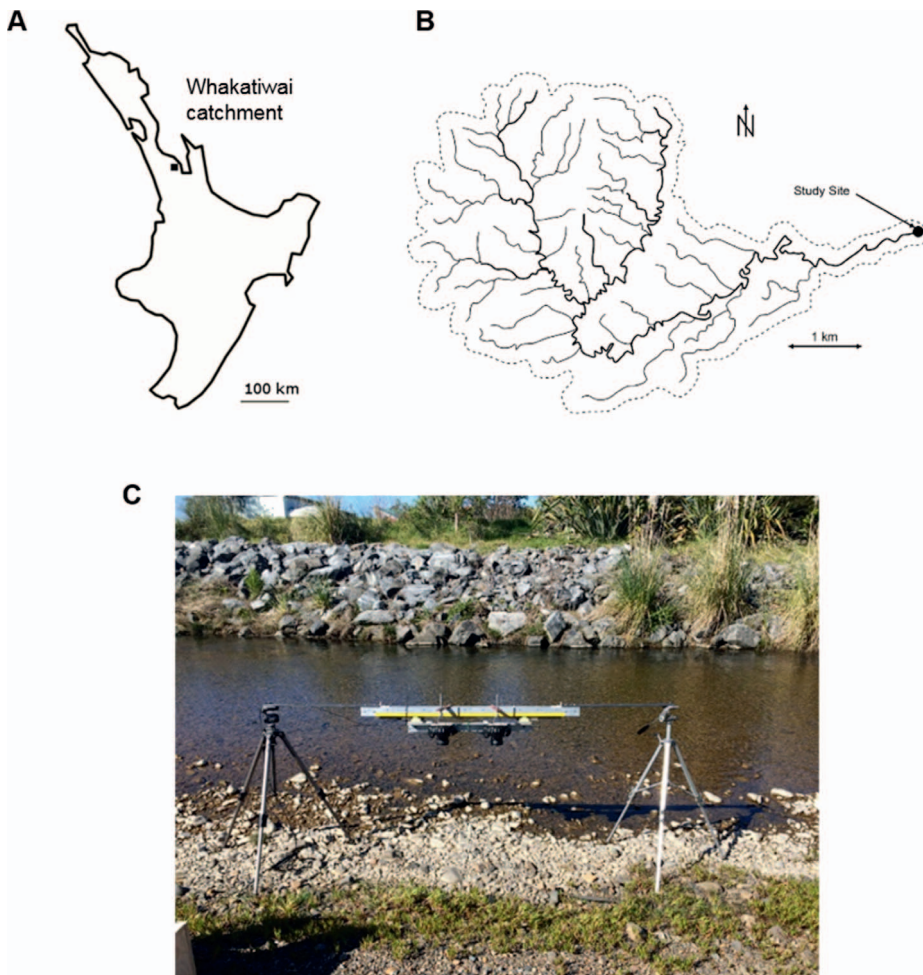


FIG. 1.—**A**) Whakatiwai catchment, located in the north east of North Island, NZ. **B**) Study site is located near the stream mouth. **C**) Photo of close-range photogrammetry setup of patches, with a rock revetment visible on the opposite bank of the stream.

for the pre-calibrated laboratory calibration. Thereby the decision was made to use the field calibration for analysis, motivated by the smaller rectification error.

Analytical Methods

Surface grain size (Table 1) was subsequently obtained through the software Basegrain[®], whereby a single photograph is used to generate a grain-size distribution for the patch (Detert and Weitbrecht 2013; Stähly et al. 2017). The minimum grain size sampled is a function of the pixel size on the gravel, with previous work indicating the need for a least 23 pixels for effective grain identification (Graham et al. 2010). With an approximate pixel size of 0.19 mm, this means that grains larger than 4.5 mm were directly accounted for using Basegrain[®]. As recommended by previous authors, measured grain-size distributions were empirically corrected, with an assumption of 10% fine sediment not accounted for during detection for all patches (as per Ruther et al. 2013). Characteristic grain sizes of the bed-surface material were determined for all patches examined (Table 1). The median grain size of the bed-surface material (d_{50}) varies between 15 mm and 25.3 mm, and the coarsest fraction of sediment (d_{90}) ranges between 32.2 mm and 64.4 mm (Table 1).

Calibration parameters necessary for accurate DEMs with photogrammetry were obtained using images of a chequerboard and Bouguet's (2010) calibration toolbox in Matlab[®], which provide both intrinsic (e.g., camera) and extrinsic (e.g., setup) parameters. Based on calibration data, obtained images of the gravel patches were rectified (maximum error < 1 pixel), through which corresponding pixels in the two overlapping images are on

the same scanline (i.e., same vertical coordinate). Stereo-matching was completed on the rectified images using Gimel'farb's (2002) symmetric dynamic programming stereo algorithm (SDPS) to produce point clouds of elevation data. Point clouds were first interpolated onto regular grids of 0.2 mm spacing, before being interpolated onto a 1 mm spacing grid (i.e., a raster DEM), resulting in less bias when calculating surface metrics in comparison to using non-uniform elevation data (Hodge et al. 2009a). Using the mean elevation difference parameter (Hodge et al. 2009b), outliers were identified and replaced using bicubic spline interpolation. DEMs were normalized to a mean bed level of zero, and subsequently rotated to align with the flow direction (Hodge et al. 2009a). Flow direction was determined by eye in the field, based on channel observations and grain imbrication (Laronne and Carson 1976; Millane et al. 2006; Bertin and Friedrich 2016). Most of each patch was vegetation free, and several overlapping DEMs were merged in order to generate patch sizes of > 1 m in length. However, in the case of some patches (e.g., bar-head site P03, and bar-center sites P06 and P07), the presence of vegetation was removed from the patch, resulting in a smaller DEM, labeled with the letter A. For P03, two DEMs were made, on either side of the vegetation, and labeled A and B. For these patches, where vegetation was present, the smaller DEMs were used for analysis.

Before surface metric calculation, DEMs were all detrended, first using a bilinear method and subsequently using a moving-window method. Bilinear detrending removes the influence of riverbed slope or experimental setup misalignments (Bertin and Friedrich 2016). Moving-window detrending removes large-scale surface distortions larger than the cluster



FIG. 2.—Images showing the evolution of the bar under investigation from A) 2015, B) 2013, C) 2010, and D) 2003. The gravel bar is highlighted by dashed black lines, and flow direction is shown by the block black arrow (in Part A), left-to-right of images. These images provide context for the bar, surrounded by farmland and densely vegetated banks. In the 2013 and 2015 images (top row), the addition of the rock revetment can be seen on the opposite bank from the bar. Source: Google Earth.

size for that patch, such as peaks and troughs resulting from bed undulations. As proposed in Smart et al. (2002), the trend surface corresponding to bed undulations was estimated over a grid with point spacing $1.25 \times d_{90}$, with the elevation of grid points measured by averaging DEM data points within a circle of diameter $2.5 \times d_{90}$ centered on the grid point, and removed from the measured DEMs before analysis. Using a

moving-window detrending method enables the grain topography to be solely considered due to the removal of bedforms, thereby subsequent roughness parameters determined from DEMs are representative of grain-scale roughness (i.e., the microtopography of the surface). Analysis of grain-scale roughness is further suitable due to the size of the patches investigated, as research has suggested that larger patch sizes may be

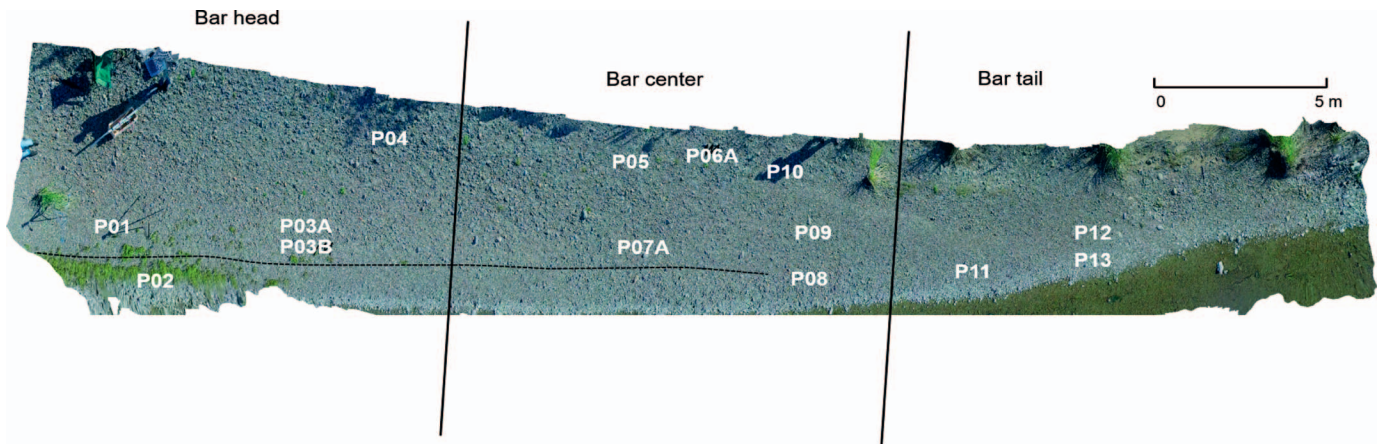


FIG. 3.—Schematic of gravel bar, overlaying an orthophoto of the bar, indicating the location of 14 measurement patches, moving down a 30 m transect downstream, and across the bar. Black dotted line represents a break in slope, and vegetation is represented schematically across the bar.

TABLE 1.—Sediment size of the surface layer for each patch studied, for d_{50} , d_{84} , and d_{90} fractions of the surface.

Patch Information				Sediment Size (mm)		
Patch	Bar location	Patch size (mm × mm)	Patch size (m ²)	d_{50}	d_{84}	d_{90}
P01	Head	1456 × 455	0.66	18.2	31.2	35.7
P02	Head	550 × 530	0.29	22.8	44.9	60.5
P03A	Head	860 × 440	0.38	20.0	33.6	37.4
P03B	Head	500 × 440	0.22	20.0	33.6	37.4
P04	Head	765 × 491	0.38	23.4	48.2	58.0
P05	Center	1704 × 408	0.69	24.0	52.3	64.4
P06A	Center	784 × 430	0.34	25.3	49.8	54.5
P07A	Center	1043 × 288	0.30	22.2	42.9	50.9
P08	Center	1848 × 384	0.71	18.3	34.4	40.2
P09	Center	1762 × 356	0.63	19.7	37.5	46.2
P10	Center	1452 × 385	0.56	22.7	48.0	56.1
P11	Tail	1518 × 412	0.63	16.5	28.2	32.8
P12	Tail	540 × 525	0.28	15.0	27.3	32.2
P13	Tail	1147 × 444	0.51	18.5	34.2	40.7

required for thorough analysis of larger-scale bed undulations (Powell et al. 2016).

Surface metrics were calculated for each patch to assess variations in surface structure across the gravel bar. First, standard deviation (σ_z) and skewness (S_k) of bed elevations were determined from probability distribution functions (Eq. 1) to characterize bed roughness (Aberle and Nikora 2006). These metrics were chosen to provide an indication of the vertical roughness length (σ_z) and water-working (S_k) (Aberle and Smart 2003; Aberle and Nikora 2006; Coleman et al. 2011; Noss and Lorke 2016). Skewness is a measure of the degree of asymmetry of the probability distribution function. Positive values are indicative of a water-worked, and armored, surface (Coleman et al. 2011; Bertin and Friedrich 2014) because of coarse grains that form the surface, and the fact that the magnitude of surface deviations below the mean is reduced by fine grains filling surface depressions (Nikora et al. 1998; Aberle and Nikora 2006).

$$\sigma_z^2 = \frac{1}{N'} \sum_{i=1}^{N'} (z_i - \langle z_i \rangle)^2 \quad (1)$$

$$S_k = \frac{1}{N' \sigma_z^3} \sum_{i=1}^{N'} (z_i - \langle z_i \rangle)^3$$

where z represents the bed elevation at location (x, y) in a DEM, N' is the total number of DEM points and $\langle \rangle$ represents the mean value.

Secondly, the inclination index (I_0) in the flow direction was calculated using Eq. 2. Here, the difference between the fraction of positive and negative slopes of particles is divided by the total number of positive, negative, and zero inclinations at a given lag (of 1 mm), which is equal to the DEM resolution. A positive slope was counted as bed elevations increasing downstream. A threshold value of ± 0.01 was set, so unreliable near-zero slopes were not calculated in the numerator of Eq. 2 (Millane et al. 2006). Particle imbrication can be inferred from positive inclination-index values, which indicates a predominance of positive slopes of the grains in the flow direction, reflecting the influence of downstream flow on the bed surface (Laronne and Carson 1976; Millane et al. 2006).

$$I_0 = \frac{n_+ - n_-}{N_s} \quad (2)$$

where n_+ and n_- are the number of positive and negative slopes between successive DEM points, respectively, and N_s is the total number of slope measurements.

The slope and aspect of individual cells of the DEMs (Eq. 3) were analyzed, using a moving window to calculate the elevations of surrounding cells, in order to provide information on the grain structures, including any preferential grain imbrication and aspect orientation; this is possible because the DEM cell size is smaller than the grain size (Hodge et al. 2009). Due to the alignment of DEMs in the flow direction, those cells with 90° aspects indicate sloping grains facing downstream and an aspect of 270° indicates sloping grains oriented upstream. Further details of the calculation of these metrics are provided in the references cited.

$$S = \arctan \sqrt{\left(\frac{dz}{dx}\right)^2 + \left(\frac{dz}{dy}\right)^2}$$

$$A = \arctan\left(\frac{dz/dx}{dz/dy}\right) \quad (3)$$

where $\frac{dz}{dx}$ and $\frac{dz}{dy}$ are the gradients in the center cell, determined from the elevations of eight perimeter cells in both the x and y direction.

Finally, second-order structure functions (2DSF) were calculated (Eq. 4) to evaluate changes in elevation correlations at differing lags and directions, which can provide an indication to surface-forming mechanisms (Nikora et al. 1998; Aberle and Nikora 2006). Gravel-bed structure functions can be separated into three regions: a scaling region with a uniform slope at small lags, a saturation region at large lags with a slope of zero, and a transition region between the two where the slope decreases (Nikora et al. 1998; Hodge et al. 2009). Small values are indicative of areas of similar elevation, and hence the same grain (as data is detrended to remove the influence of bedforms), and once values are saturated they indicate that elevations are no longer correlated. Second-order structure functions are displayed in 2D isopleth maps, which allow the identification of the length and spatial arrangement of surface layer features (Bertin et al. 2017), and horizontal roughness lengths can be calculated in both the streamwise and cross-stream directions (L_x and L_y). Horizontal roughness lengths L_x and L_y are calculated from the breakpoint in the slope between the scaling region and the saturation region of the 1D structure functions for $\Delta x = 0$ and $\Delta y = 0$, respectively.

$$D_{G2}(\Delta x, \Delta y) = \frac{1}{(N-n)(M-m)} \sum_{i=0}^{N-n} \sum_{j=0}^{M-m} \{z(x_i + n\delta x, y_j + m\delta y) - z(x_i, y_j)\}^2 \quad (4)$$

where $\Delta x = n\delta x$ and $\Delta y = m\delta y$; δx and δy are the sampling intervals (i.e.,

DEM resolution) in the longitudinal and transverse directions respectively; $n = 1, 2, 3, \dots, N$ and $m = 1, 2, 3, \dots, M$, N , and M are the number of DEM points in the same two directions.

RESULTS

Roughness parameters were calculated with both distance down bar and distance from the water edge (Fig. 4), in order to assess down-bar and lateral variability in surface structure and grain size.

Whereas there is no simple correlation of roughness parameters with distance down bar and from the water edge (i.e., low R^2 values and significant scatter in the data), there are patterns of a reduction in surface sediment size (both d_{50} and d_{90} fractions of the surface) with distance down bar, compared to an increase with distance from the water edge. There is more scatter in data for d_{90} values due to the wider range in sediment size measured across the patches (as seen in Table 1, where values vary from 32 mm to 65 mm). Following the pattern observed in sediment size, the standard deviation of elevations (σ_z) decreases with distance down bar and increases with distance from water edge. These patterns can be seen qualitatively across patch surfaces, in particular a visible reduction in grain size at the downstream and water-edge patches (Fig. 5).

In contrast to these patterns, skewness increases with both distance down bar and distance from the water edge. The majority of patches have positive skewness values, aside from P02 (bar head), which has a negative skewness ($S_k = -0.0971$).

For both the inclination index and horizontal roughness lengths, the pattern follows that of sediment size and standard deviation of elevations, whereby each roughness parameter decreases down bar and increases with distance from the water edge. Therefore, consistencies in patterns of the roughness parameters are evident (Fig. 4), aside from skewness, which differs from the other roughness parameters.

Although there are these patterns in roughness parameters with distance down bar and from the water edge (Fig. 4), there is significant scatter in the data, largely due to the complex topography of the gravel surface. This scatter, and with low Pearson's coefficients of determination (R^2) for the relations, is indicative of spatial variability in roughness statistics at the bar scale and reflects complex sedimentation patterns at this scale. The coefficients of determination for those roughness parameters for distance from the water edge are higher than those for distance down bar. This suggests a more robust relationship between distance and roughness statistics in a lateral direction, which has important implications for field data collection since such patterns are rarely explored.

Further results (Fig. 6) confirm a decrease in the median value of roughness parameters towards the bar tail for all parameters (e.g., sediment size, σ_z , inclination index, and horizontal roughness lengths), except skewness, which displays an increase with distance down bar. There are also consistent decreases in the spread of data (variance in roughness statistics) towards the bar tail.

At the downstream end of the bar, median σ_z is 30% lower than the bar-head values, consistent with fine grain sizes constituting the surface, as evident in the trends of reduced d_{50} , d_{90} and σ_z with distance down bar (Figs. 4, 6). These patterns are in accordance with field results from the Fraser River, where a 33% reduction in median grain size from the bar head to the bar tail was documented (Rice and Church 2010). For our results, the mean values of the bar head and bar tail were compared using t-tests with a 95% confidence level, and were found to be statistically different for d_{50} , σ_z , and inclination index. There were significant differences between the bar center and the bar tail for all parameters, except skewness. All roughness parameters were found to be statistically similar between the bar head and bar center.

The surface slope and aspect are presented as polar plots for all patches and overlaid on an enlarged schematic of the bar (Fig. 7). Flow is assumed to be from left to right in polar plots (i.e., from 270° to 90°). For all

patches, the majority of aspects are upstream (around 270°), particularly on patches upstream of the bar (including P01, P04, P05, P06, and P07). Patches P08–P13 (bar center and bar tail) have a higher density of upstream aspects, but they also have more downstream aspects than those patches upstream. These observations of accentuated particle imbrication at the bar head compared to the bar tail follow previous results showing a reduction in inclination index at the bar tail (Fig. 6D). Further, the slopes of DEM cells (assumed to be grains) can be assessed. The highest slopes observed are about 80° (Fig. 7), and these are positioned predominantly perpendicular to the flow. Visually, this is shown by shaded areas going farther away towards the circles' edges for 0° and 180° aspect angles (Fig. 7). This is more evident in patches P09–P13 (bar center and bar tail) at the downstream end of the bar.

Examining the relationship between multiple roughness parameters and grain size provides a baseline for future studies. For our results, the strongest correlation exists between roughness lengths in the downstream direction (L_x) and d_{90} (Fig. 8). Roughness parameters, except skewness and d_{90} have correlations ranging between $R^2 = 0.47$ and 0.88 . Relationships between roughness parameters and d_{50} also display strong correlations ($R^2 = 0.71$ – 0.85) (Fig. 8). The exception, skewness, shows weak correlation ($R^2 = 0.27$ and $R^2 = 0.21$ for d_{50} and d_{90} respectively). Even with the removal of the one anomalous site (P02, which has a negative skewness) the relationship is still below that of other roughness parameters ($R^2 = 0.35$ and $R^2 < 0.1$ for d_{50} and d_{90} , respectively).

DISCUSSION

Assessing Within-Bar Variability in Surface Roughness

The assessment of σ_z is an improvement on the former technique of using grain size as a roughness parameter, as gravel beds with similar grain sizes can have contrasting σ_z values (Cooper and Tait 2009; Hodge et al. 2009). The pattern of higher σ_z values (i.e., indication of a rougher surface, Fig. 6B) upstream of the bar, at the bar head, and bar center, partly denotes coarser grains that have accumulated at these sites (Fig. 6A). Our observations of within-bar variability are attributed to varying locations and elevations on the bar. More specifically, field observations and an orthophoto (Fig. 3) indicate that upstream patches are elevated relative to the water line compared to patches at the bar tail, and may therefore be exposed for all but the highest flows, whereas patches at the bar tail are more frequently submerged. The pattern of upstream patches with larger sediment sizes and σ_z is comparable to patterns observed in laboratory studies, and is thought to reflect a coarse armor layer that formed as a result of higher discharges (Aberle and Nikora 2006). Contrasting roughness properties for patches at the bar tail may be due to exposure to more frequent sediment transport events and to submergence during lower flows. Differences in patch elevation on the bar also influence the distribution of bed shear stress during submergence, with higher bed shear stress occurring in areas on the bar top, due to higher velocities and reduced water depths. Previous experimental work showed an increase in surface roughness with shear stress, which is relevant to this study (Aberle and Nikora 2006). Further, data from Rice and Church (2010) showed that varying bar elevation determines shear-stress distribution across the bar, which in turn determines the sediment size distribution.

Whereas the patches at the water edge are more frequently submerged by flows and contain smaller grain sizes, those patches nearer the bank of the river are more stable and have coarser sediment (Fig. 4, higher d_{50} and σ_z). This suggests that these areas experience high flow events (and are otherwise exposed), which winnow fine sediment and move the coarse sediment infrequently (Leopold and Wolman 1957). For the majority of patches on this bar, skewness values are positive, representing water-working across the bar, except patch P02 at the bar head (Fig. 4), which has a negative skewness value. This patch, located below the change in

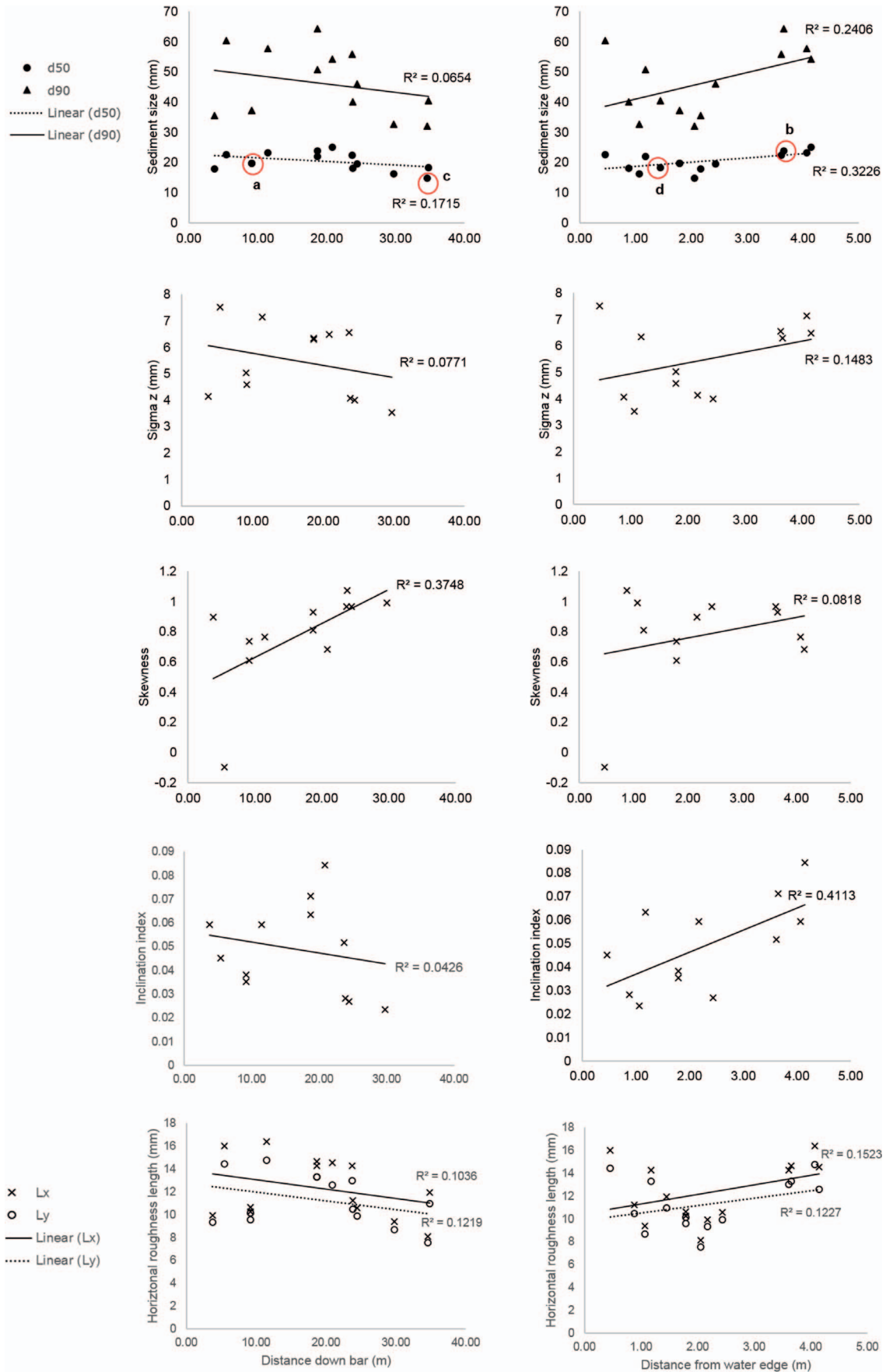


FIG. 4.—Roughness statistics (including sediment size, standard deviation of elevations, skewness, inclination index, and horizontal roughness lengths) with distance down bar and distance from the water edge for all 14 patches measured. Circled data points in the top graphs and associated labels refer to figure labels in Figure 5.

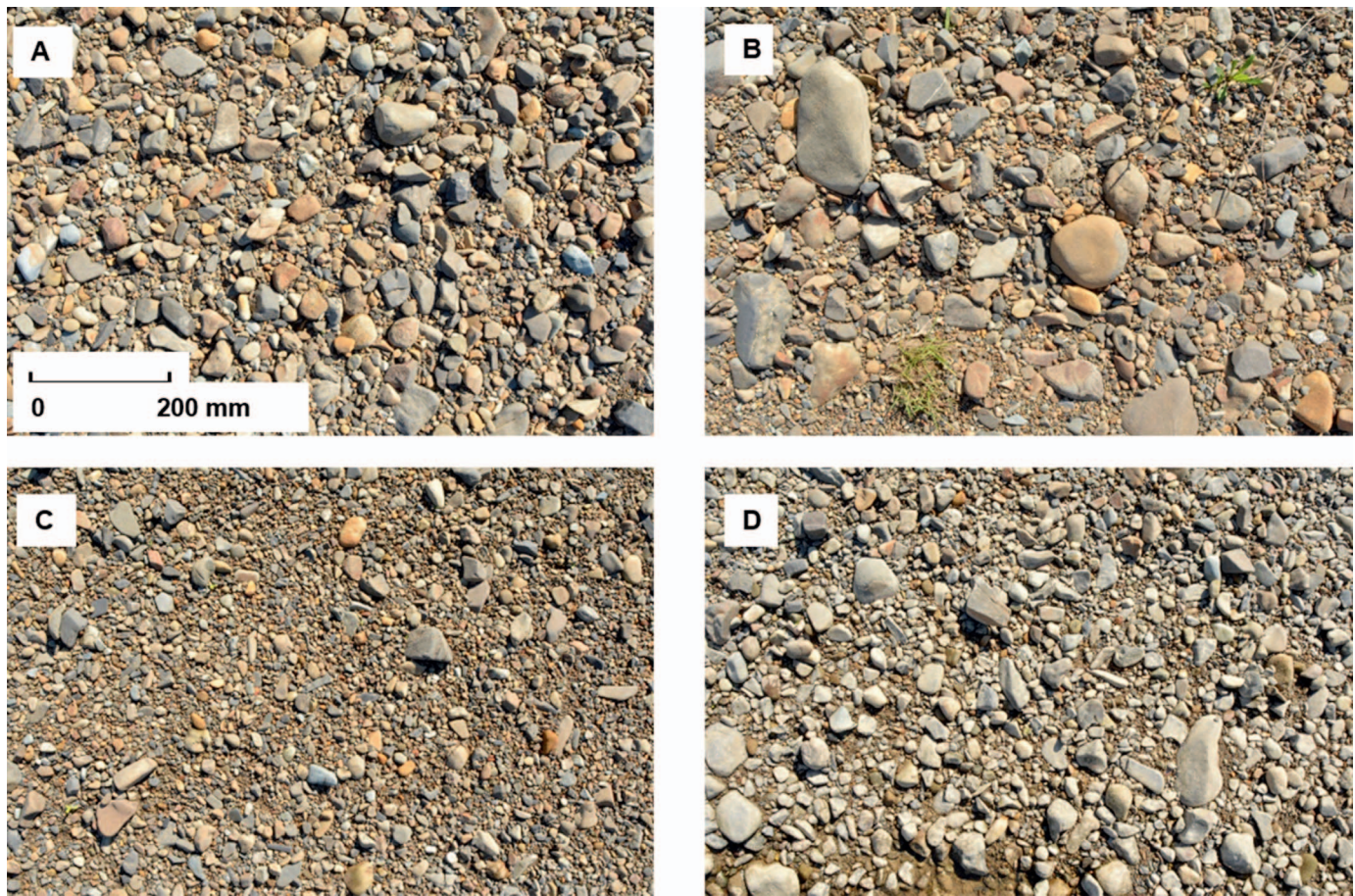


FIG. 5.—Photographs of grain size **A**) at upstream patch P03A, **B**) away from the water edge P05, **C**) downstream P12, and **D**) at the water edge P13. All photographs are the same size and were taken from the same height above the bed. The grain-size data for these patches are circled and labeled in Figure 4.

elevation (i.e., below the bar platform), near vegetation, could explain its singularity. The trend of increasing skewness with distance down bar is the opposite of other roughness parameters (Figs. 4, 6), with the patches at the bar tail having higher skewness values, suggestive of fewer surface depressions from the deposition of fine sediment in any gaps between coarse sediment during subaqueous transport (Nikora et al. 1998; Aberle and Nikora 2006).

All patches have positive inclination index values, indicating grain imbrication across the bar (Hodge et al. 2009; Qin and Ng 2012). This is consistent with the findings of Rice and Church (2010), who found that only two out of 87 of their locations displayed no evidence of imbrication. All of their locations were on primary and secondary unit bars, although the locations of the non-imbricated surfaces in the bars were not defined. Here, higher values of inclination index at the bar head and near the bank (Figs. 4, 6) suggest greater imbrication of particles and a higher degree of packing (Cooper and Tait 2009), and therefore sediment is more stable and less readily available for transport. Previous work has related grain imbrication to the movement of the coarse grains on the bed by rolling and sliding (Larone and Carson 1976), as those grains can stack against each other after meeting with an obstacle, forming imbricated grain structures. In contrast, the bar tail and the water edge have particles that may be more easily repositioned in future flow events due to the surface being poorly organized (Mao et al. 2011). Although values of inclination index can provide information with regard to the imbrication of a surface, it is useful to combine this with the analysis of slope and aspect (Fig. 7), as this can determine the slope values of grains (Qin and Ng 2012).

Analysis of surface slope and aspect of DEM cells in polar plots (Fig. 7) has been used in only a few gravel-bed river studies to date (Hodge et al. 2009; Qin and Ng 2012; Bertin and Friedrich 2016). Along with calculations of inclination index, this method is more quantitative than previous assessments of imbrication in the field. Imbrication was previously assessed and categorized qualitatively, to extract information regarding the degree of reworking and mobility of grains, with 38% of locations classified as weakly imbricated and 60% of locations classified as strongly or very strongly imbricated (Rice and Church 2010). For all our patch locations (Fig. 7), there is a majority of upstream aspects (i.e., high density of points around 270°), which is consistent with our previous observations of grain imbrication in a direction parallel to the flow using the inclination index (Hodge et al. 2009; Qin and Ng 2012). If imbrication is observed in a single direction, this can confirm the assumed flow direction from field observations (Bertin and Friedrich 2016), which in this study is true (Fig. 7), where flow was assumed to be from 270 to 90° .

Our results quantitatively affirm previous geomorphological results. Although spatial variability within bars is of no surprise, as geomorphologists and sedimentologists frequently gather data from a consistent location (i.e., the bar head) when making inter-bar comparisons of surfaces (Rice and Church 2010), our study emphasizes that a single sample from one exposure cannot represent the whole gravel-bar surface. This has important implications for the development of a standardized sampling approach, and for the selection of roughness parameters in models, which is difficult due to the displayed complexity (i.e., variability) of roughness at the bar scale (Rice and Church 2010). Our empirical findings of variations

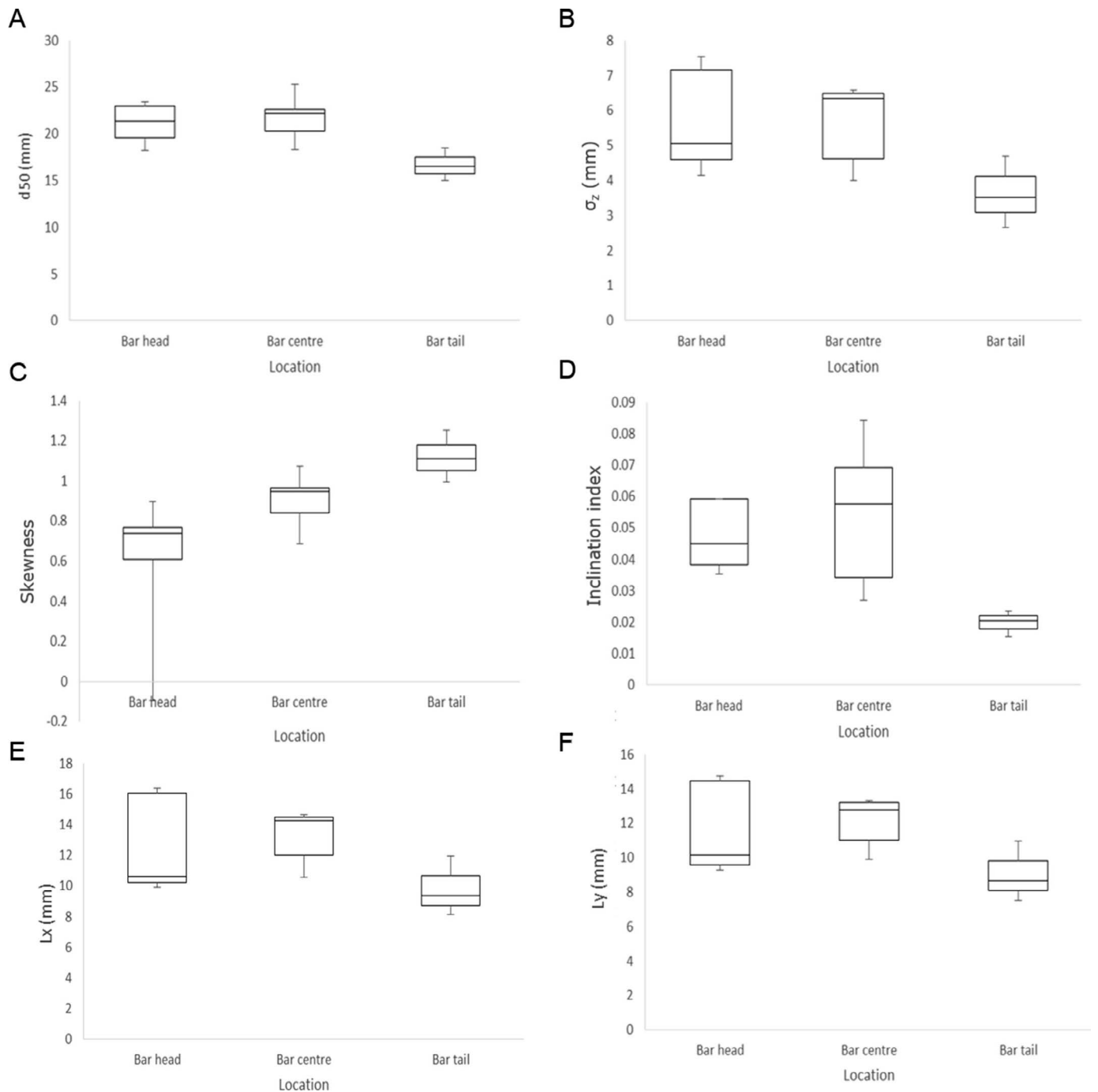


FIG. 6.—Boxplots of roughness statistics: d_{50} , σ_z , skewness, inclination index, horizontal roughness length L_x , and horizontal roughness length L_y , for three locations of the bar (sample size $n = 5$ for bar head, $n = 6$ for bar center, and $n = 3$ for bar tail). The horizontal line in the boxplot represents the median value for each location, the upper and lower box limits represent the 75% and 25% percentiles respectively, and whiskers display the range in values.

in roughness across a gravel bar can be used to validate and calibrate flow-resistance equations and morphodynamic models, including comparisons of model predictions with field data (Rice and Church 2010; Powell 2014).

Examining Roughness Relationships with Grain Size

Throughout research, three roughness metrics are commonly used, as summarized in Pearson et al. (2017): (i) roughness height (rh) (Vazquez-Tarrio et al. 2017), which is the difference in height between the top of the

particle and the averaged topographic surface (i.e., mean-bed elevation); (ii) twice the standard deviation of elevations (Heritage and Milan 2009); and (iii) root-mean-square height (RMSH), the standard deviation of heights in a given area for which the average slope has been detrended (Vazquez-Tarrio et al. 2017).

Pearson et al. (2017) summarizes published R^2 values for grain size versus topographic elevation for fluvial systems only, and there is a range between 0.231 and 0.96, although 50% of studies provide a strong relationship that exceeds $R^2 = 0.8$. Vazquez-Tarrio et al. (2017) found

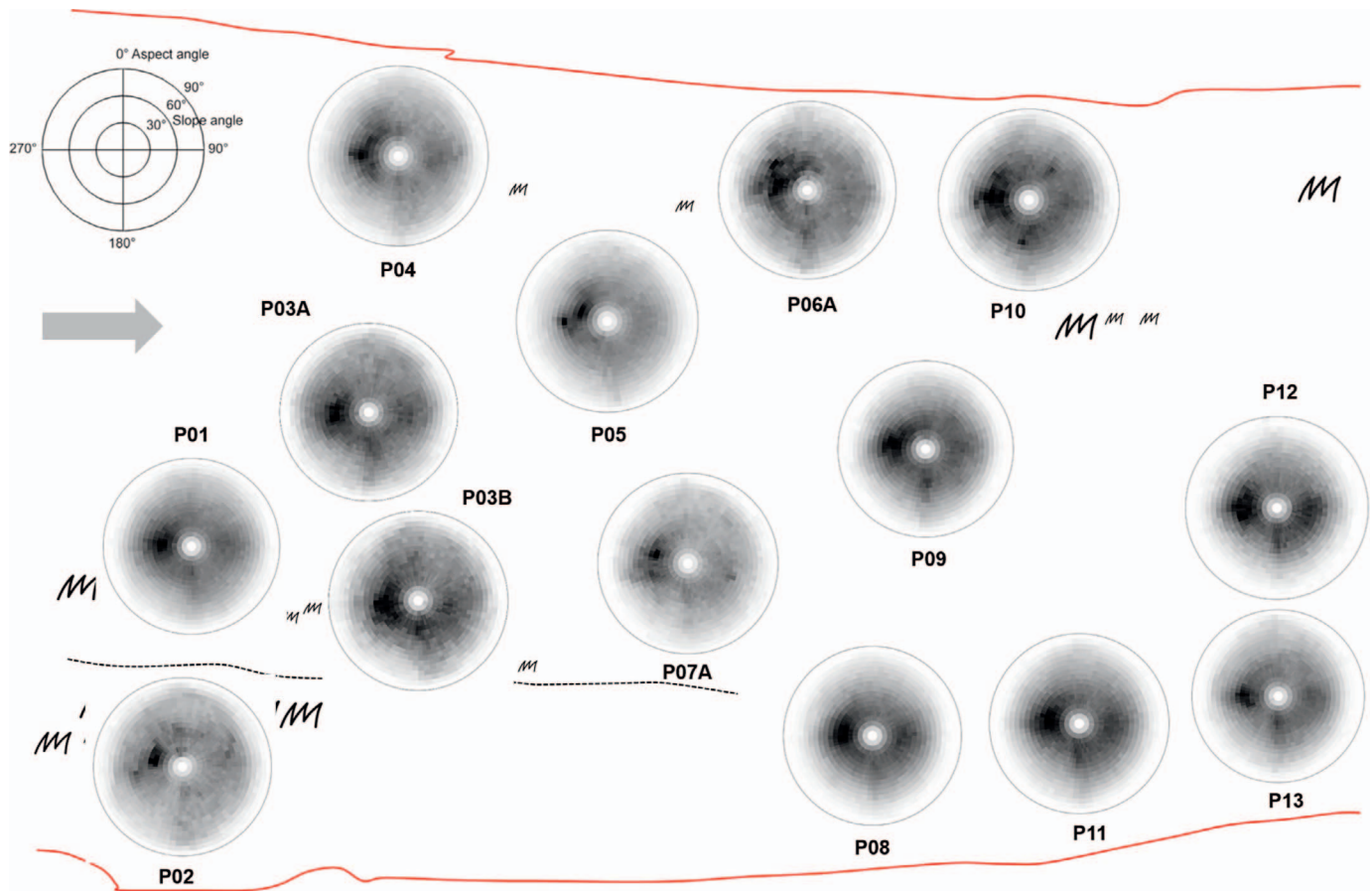


Fig. 7.—Surface slope and aspect polar plots, presented on an enlarged schematic of the bar (as per Fig. 3) to enable location of patch to be identified. Flow is assumed from left to right (gray arrow). Aspect angle is from 0 to 360°, and slope angle is from 0 to 90°, with high density of points shaded black, and low density of points shaded white. Black dotted line represents a break in slope, and vegetation is represented schematically. Note that the placement of polar plots is not to scale.

moderate to strong correlations for all roughness metrics ($R^2 = 0.45\text{--}0.90$) between surface roughness and truncated grain size (< 8 mm were removed). The best correlation was with rh , and the weakest fit with RMSH.

To our knowledge, this is the first time the relationship between the studied roughness parameters (e.g., inclination index or horizontal roughness lengths) and grain size have been investigated (Fig. 8). The data on multiple roughness parameters and d_{50} in this study (Fig. 8) yield R^2 values between 0.71 and 0.85, which lie in the range of published values (Pearson et al. 2017; Vazquez-Tarrio et al. 2017). The one exception is skewness, which has a weak correlation ($R^2 = 0.27$) with grain size. Although skewness cannot be a proxy for grain size, it can contribute to the understanding of a surface (e.g., degree of water-working).

Case studies indicate that there are different relationships between surface roughness and grain size, reflecting different surface textural characteristics (Pearson et al. 2017; Vazquez-Tarrio et al. 2017). Further, patches with similarities in grain size have distinct roughness differences due to packing, burial, and imbrication (Heritage and Milan 2009; Hodge et al. 2009). There needs to be more data (including that of various roughness parameters) on differing sediment textures, to determine roughness and grain-size relationships.

Inferring Sedimentation Patterns from Roughness Parameters

The gravel bar studied in this paper is a channel side bar, or lateral bar, in a non-meandering section of the channel. Lateral channel bars attach to

one bank, in a narrow section of the channel, and sediment accumulates at both ends of the bar (Church and Jones 1982).

Evidence of down-bar decreases in sediment size, σ_z , and inclination index (Figs. 4, 6) implies down-bar fining in sediment. Bar heads are thought to have formed during high flows (Leopold and Wolman 1957; Bluck 1976). Due to an inability of subsequent lower flows to transport the coarse sediment, it remains *in situ* (Leopold and Wolman 1957; Bluck 1976; Francalanci et al. 2012). The coarse sediment becomes the nucleus for bar development, by modifying local flow structures and creating local turbulence that leads to winnowing of fine sediment. Further, fine sediment is trapped at the margins of the bar and is moved downstream during a range of flow rates (Leopold and Wolman 1957; Nanson 1980; Bluck 1982; Leopold 1992; Ashworth 1996; Parker 2008).

From field observations, there is a well-defined bar platform across the studied bar (Fig. 3) with dense vegetation (pampas grass) on top (Blacknell 1982). The junction between a channel and the bar platform is known as an avalanche face, and these can range between a few centimeters to a few meters high (Blacknell 1982; Rice et al. 2009). In the case of this bar, the avalanche face is approximately 1 meter high.

Due to the presence of a bar platform, the patches located at higher elevations (i.e., on the bar platform), and away from the water edge are strongly armored, with increased sediment size and σ_z . A tentative correlation between surface elevation (or bar thickness) and surface sediment size has previously been made, and this apparently contributes to deviations in reach-scale downstream fining trends (Rice and Church 2010). In comparison, those patches at the water edge appear to be

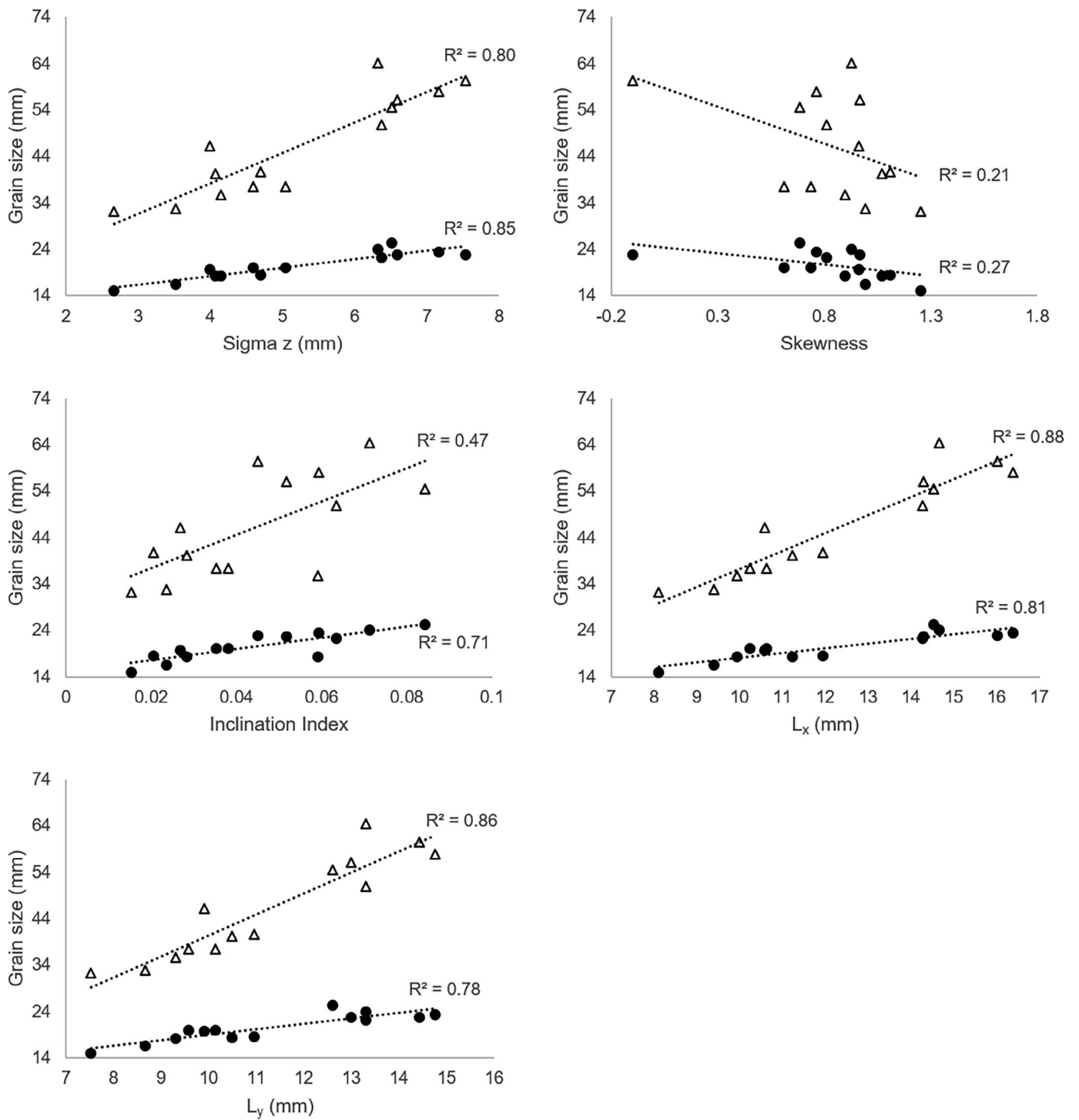


FIG. 8.—Roughness relationships for standard deviation of elevations, skewness, inclination index, and horizontal roughness lengths with grain size. Circles represent d_{50} grain size, and open triangles represent the d_{90} grain size.

undergoing multiple erosion and deposition cycles, and sediment accumulates there due to lateral accretion of fine grains (Bluck 1982) (Fig. 9A). Downstream of the bar and bar platform, finer sediment is evident (reflected in a decrease in grain size and σ_z in Figs. 4 and 6). Along with lateral accretion, this could be due to the bar tail becoming a shadow zone during high flows (Fig. 9B). This depositional mechanism occurs as fine sediment is transported over the bar platform until

subsequent falling flow stages result in the deposition of the sediment at the bar tail (Leopold and Wolman 1957; Burge 2006; Rice and Church 2010). The lateral accretion of sediment is substantiated by field observations of lighter-colored sediment located below the bar platform near the water edge (e.g., P02), indicating that it has been deposited more recently than the stable, darker sediment on the bar platform. Furthermore, increases in roughness parameters with distance from the

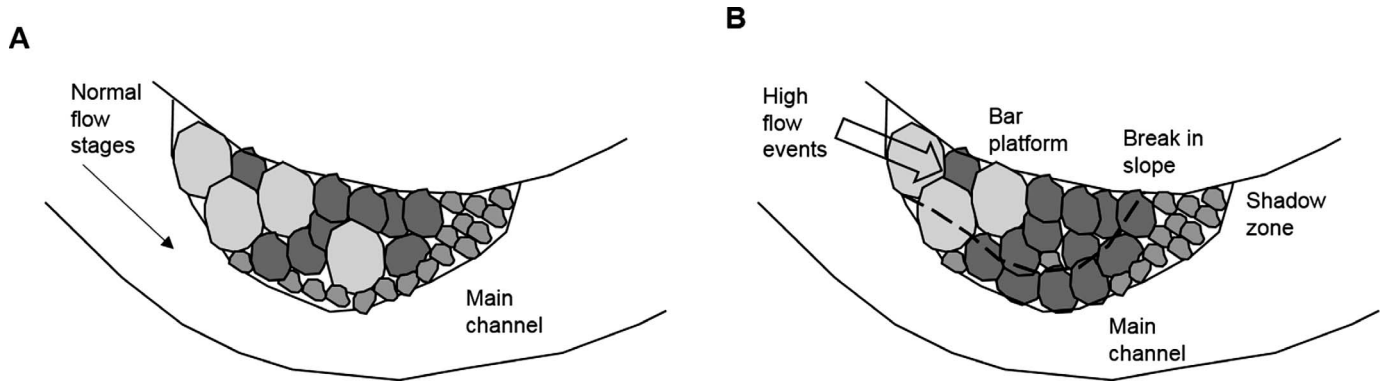


FIG. 9.—Schematic of sedimentation patterns occurring on this bar. **A**) Lateral accretion, whereby fine sediment is deposited at the edge of the bar and downstream. **B**) Down-bar fining due to sediment being transported over the bar platform during high flows and deposited in the shadow zone during the falling limbs of hydrographs.

water edge (Fig. 4), supports the idea that the bar is undergoing lateral accretion of sediment.

The scatter in our data (Fig. 4) suggests that the bar is complex in nature, with secondary sedimentation patterns, supporting observations made from historical images (Fig. 2) that demonstrate downstream propagation of the bar and provide evidence for cycles of erosion and deposition (Rice and Church 2010). Furthermore, sedimentation patterns on this bar may be difficult to interpret due to larger morphological features in the river channel at this location. Directly opposite this bar is a rock revetment, which was installed *circa* late 2011 (Hauraki Council Report 2011). In natural river channels, deposition of sediment (e.g., on exposed gravel bars) is compensated for by erosion of the opposite bank, in order for the channel to maintain conveyance (Rice and Church 2010). However, in this case sediment deposition cannot be compensated for directly opposite the bar, which thus influences the flow and natural sedimentation patterns.

An improved understanding of the variability in bed roughness is beneficial for modeling purposes, and for interpretations of sedimentation patterns and morphology. These are important for successful river restoration procedures and the management of natural systems. The Whakatiwai River studied has at times flooded local communities, and local people have called for effective management to be put in place to protect sacred cultural sites (Hauraki District Council 2011). Therefore, developing and improving the understanding of sedimentation patterns can guide management strategies in the future, which is applicable to other locations around the globe.

Further, roughness properties can be measured between flow events to provide a signature of erosional and depositional processes (Smith 2014). Previous research has not established a direct association between changes in grain size and morphological change (Rice and Church 2010; Vazquez-Tarrio et al. 2017). However, we suggest that applying the technique presented in this manuscript multiple times (i.e., following flow events) can aid in the detection of temporal changes in roughness and help to relate changes in roughness to morphological changes. This could involve the installation of GPS markers in order to identify where the patch locations were for repeat surveys.

CONCLUSION

This study investigated intra-bar variability in roughness statistics across a bar at 14 patch locations extending 35 m down bar and 5 m across the bar from the water edge. This extends previous work that focused on grain size and qualitative estimates of parameters such as imbrication. Data were collected using close-range photogrammetry, a technology used for the first time to assess intra-bar variations of surface roughness.

Roughness statistics were found to vary across the bar, with evidence of down-bar reductions in grain size, changes in standard deviation of elevations, imbrication of particles, variations in horizontal roughness lengths, and an increase in skewness down bar. This paper therefore provides quantification of earlier observations of sorting across a bar. There is a stronger correlation of increased roughness with distance from the water edge. This lateral variation of roughness and sedimentation patterns across gravel bars is infrequently documented, compared to down-bar patterns, but it is an important consideration for a wide range of fluvial studies, including river restoration. It is also important for choosing a location in the field to measure roughness properties. Relationships between roughness parameters and grain size (d_{50}) were examined, and strong correlations ($R^2 = 0.71\text{--}0.85$) were found in all parameters except skewness. Assessing the relationship between roughness parameters and grain size is timely, as previously no universal relationship has been found, suggesting that grain size cannot be used as a proxy for surface roughness.

Following on previous photogrammetry and laser-scanning studies, this study infers sedimentation patterns from roughness statistics, with the consideration of wider morphological influences. The trends observed in this study are indications of sediment deposition at the bar tail and the water edge, and coarse stable sediment at the bar head and near the banks of the bar, which are consistent with lateral accretion. Inferring sedimentation patterns from these roughness statistics can be difficult due to scatter in the data, highlighting the complexity of surface roughness, resulting from several cycles of erosion and deposition. Understanding these sedimentation patterns in the Whakatiwai River, and other rivers, is needed for the successful implementation and monitoring of river management.

This paper has highlighted the variability in roughness statistics across a gravel bar and the benefit of using a range of surface metrics to corroborate observations. Future work that would benefit geomorphologists includes the assessment of roughness parameters at a larger scale (i.e., to include the effect of bedforms), quantification of roughness parameters on multiple bars in different river systems, assessments of roughness over temporal scales, and identifying if a single roughness parameter can be used to represent larger-scale roughness. This would assist in the development of gaining appropriate roughness parameters for flow resistance, morphodynamic, and empirical models.

ACKNOWLEDGMENTS

We would like to thank Wei Li and Trevor Patrick for assistance in acquiring the data and Wei Li for preparing the orthophoto in Figure 3. The study was partly funded by the Marsden Fund (Grant No. UOA1412), administered by the Royal Society of New Zealand. Anonymous reviews and the insightful feedback from Dr. Paul Myrow are greatly appreciated.

REFERENCES

- ABERLE, J., AND SMART, G., 2003, The influence of roughness structure on flow resistance on steep slopes: *Journal of Hydraulic Research*, v. 41, p. 259–269.
- ABERLE, J., AND NIKORA, V., 2006, Statistical properties of armored gravel bed surfaces: *Water Resources Research*, v. 42, W11414.
- ASHWORTH, P., AND FERGUSON, R., 1986, Interrelationships of channel processes, changes and sediments in a proglacial braided river: *Geografiska Annaler*, v. 68A, p. 361–371.
- ASHWORTH, P.J., 1996, Mid-channel bar growth and its relationship to local flow strength and direction: *Earth Surface Processes and Landforms*, v. 21, p. 103–123.
- BAEWERT, H., BIMBÖSE, M., BRYK, A., RASCHER, E., SCHMIDT, K., AND MORCHE, D., 2014, Roughness determination of coarse grained alpine river bed surfaces using terrestrial laser scanning data: *Zeitschrift für Geomorphologie*, v. 58, p. 81–95.
- BERTIN, S., AND FRIEDRICH, H., 2014, Measurement of gravel-bed topography: evaluation study applying statistical roughness analysis: *Journal of Hydraulic Engineering*, v. 140, p. 269–279.
- BERTIN, S., AND FRIEDRICH, H., 2016, Field application of close-range digital photogrammetry (CRDP) for grain-scale fluvial morphology studies: *Earth Surface Processes and Landforms*, v. 41, p. 1358–1369.
- BERTIN, S., GROOM, J., AND FRIEDRICH, H., 2017, Isolating roughness scales of gravel-bed patches: *Water Resources Research*, v. 53, p. 6841–6856.
- BERTOLDI, W., ZANONI, L., MIORI, S., REPETTO, R., AND TUBINO, M., 2009, Interaction between migrating bars and bifurcations in gravel bed rivers: *Water Resources Research*, v. 45, p. 1–12.
- BLACKNELL, C., 1982, Morphology and surface sedimentary features of point bars in Welsh gravel-bed rivers: *Geological Magazine*, v. 119, p. 181–192.
- BLUCK, B., 1976, Sedimentation in some Scottish Rivers of Low Sinuosity: *Royal Society of Edinburgh, Transactions*, v. 69, p. 425–456.
- BLUCK, B., 1982, Texture of gravel bars in braided streams, in Hey, R., Bathurst, J., and Thorne, C., 1982, *Gravel Bed Rivers*: Chichester, John Wiley and Sons, p. 339–356.
- BOUGUET J.-Y., 2010, http://www.vision.caltech.edu/bouguetj/calib_doc/.
- BRASINGTON, J., VERICAT, D., AND RYCHKOV, I., 2012, Modeling river bed morphology, roughness and surface sedimentology using high resolution terrestrial laser scanning: *Water Resources Research*, v. 48, p. 1–18.
- BURGE, L., 2006, Stability, morphology and surface grain size patterns of channel bifurcation in gravel-cobble bedded anabranching rivers: *Earth Surface Processes and Landforms*, v. 31, p. 1211–1226.
- CARBONNEAU, P., LANE, S., AND BERGERON, N., 2004, Catchment-scale mapping of surface grain size in gravel bed rivers using airborne digital imagery: *Water Resources Research*, v. 40, p. 1–11.
- CHURCH, M., 2006, Bed material transport and the morphology of alluvial river channels: *Annual Review of Earth and Planetary Sciences*, v. 34, p. 325–354.
- CHURCH, M., AND JONES, D., 1982, Channel bars in gravel-bed rivers, in Hey, R., Bathurst, J., and Thorne, C., 1982, *Gravel Bed Rivers*: Chichester, John Wiley and Sons, p. 291–338.
- COLEMAN, S.E., NIKORA, V.I., AND ABERLE, J., 2011, Interpretation of alluvial beds through bed-elevation distribution moments: *Water Resources Research*, v. 47, W11505.
- COOPER, J., AND TAIT, S., 2009, Water-worked gravel beds in laboratory flumes: a natural analogue?: *Earth Surface Processes and Landforms*, v. 34, p. 384–397.
- CURRAN, J., AND WATERS, K., 2014, The importance of bed sediment sand content for the structure of a static armor layer in a gravel bed river: *Journal of Geophysical Research*, *Earth Surface*, v. 119, p. 1484–1497.
- DEPERT, M., AND WEITBRECHT, V., 2013, Automatic object detection to analyze the geometry of gravel grains: a free stand-alone tool: *Advances in Science and Research*, p. 1789–1795.
- ENWISTLE, N., AND FULLER, I., 2009, Terrestrial Laser scanning to derive the surface grain size facies character of gravel bars, in Heritage, G., and Large, A., 2009, *Laser Scanning for the Environmental Sciences*: Sussex, Blackwell Publishing, p. 102–114.
- FERGUSON, R., 2010, Time to abandon the Manning equation?: *Earth Surface Processes and Landforms*, v. 35, p. 1873–1876.
- FRANCLANCI, S., SOLARI, L., TOFFOLON, M., AND PARKER, G., 2012, Do alternate bars affect sediment transport and flow resistance in gravel-bed rivers?: *Earth Surface Processes and Landforms*, v. 37, p. 866–875.
- GIMEL'FARB, G., 2002, Probabilistic regularisation and symmetry in binocular dynamic programming stereo: *Pattern Recognition Letters*, v. 23, p. 431–442.
- GRAHAM, D.J., ROLLET, A., PIÉGAY, H., AND RICE, S.P., 2010, Maximizing the accuracy of image-based surface sediment sampling techniques: *Water Resources Research*, v. 46.
- HARDY, R., 2006, Fluvial geomorphology: Progress in Physical Geography, v. 30, p. 553–567.
- HAURAKI DISTRICT COUNCIL, 2011, Drainage Manager's Report on Kaiua Issues, October 2011, File reference 819 756, Accessed December 2016.
- HERITAGE, G., AND MILAN, D., 2009, Terrestrial laser scanning of grain roughness in a gravel bed river: *Geomorphology*, v. 11, p. 4–11.
- HODGE, R., BRASINGTON, J., AND RICHARDS, K., 2009a, Analyzing laser-scanned digital terrain models of gravel bed surfaces: linking morphology to sediment transport processes and hydraulics: *Sedimentology*, v. 56, p. 2024–2043.
- HODGE, R., BRASINGTON, J., AND RICHARDS, K., 2009b, In situ characterisation of grain-scale fluvial morphology using terrestrial laser Scanning: *Earth Surface Processes and Landforms*, v. 34, p. 954–968.
- LARONNE, J., AND CARSON, M., 1976, Interrelationships between bed morphology and bed-material transport for a small, gravel-bed channel: *Sedimentology*, v. 23, p. 67–85.
- LEOPOLD, L., 1992, Sediment size that determines channel morphology, in Billi, P., Hey, R., Thorne, C., and Tacconi, P., 1992, *Dynamics of Gravel-Bed Rivers*: John Wiley and Sons, p. 297–311.
- LEOPOLD, L., AND WOLMAN, M., 1957, River channel patterns: braided, meandering and straight: U.S. Geological Survey, Professional Paper, 282B, p. 39–85.
- MAO, L., COOPER, J., AND FROSTICK, L., 2011, Grain size and topographical differences between static and mobile armor layers: *Earth Surface Processes and Landforms*, v. 26, p. 1321–1334.
- MILAN, D., HERITAGE, G., AND HETHERINGTON, D., 2007, Application of a 3D laser scanner in the assessment of erosion and deposition volumes and channel change in a proglacial river: *Earth Surface Processes and Landforms*, v. 32, p. 1657–1674.
- MILLANE, R., WEIR, M., AND SMART, G., 2006, Automated analysis of imbrication and flow direction in alluvial sediments using laser-scan data: *Journal of Sedimentary Research*, v. 76, p. 1049–1055.
- NANSON, G., 1980, Point bar and floodplain formation of the meandering Beaton River, northeastern British Columbia, Canada: *Sedimentology*, v. 27, p. 3–29.
- NIKORA, V.I., GORING, D.G., AND BIGGS, B.J., 1998, On gravel-bed roughness characterization: *Water Resources Research*, v. 34, p. 517–527.
- NOSS, C., AND LORKE, A., 2016, Roughness, resistance, and dispersion: relationships in small streams: *Water Resources Research*, v. 52, p. 2802–2821.
- PARKER, G., 2008, Chapter 3: Transport of gravel and sediment mixtures, in Garcia, M., ed., *Sedimentation Engineering: Processes, Measurements, Modeling and Practice*: American Society of Civil Engineers, p. 165–251.
- PEARSON, E., SMITH, M., KLAAR, M., AND BROWN, L., 2017, Can high resolution 3D topographic surveys provide reliable grain size estimates in gravel bed rivers?: *Geomorphology*, v. 293, p. 143–155.
- POWELL, M., 2014, Flow resistance in gravel-bed rivers: progress in research: *Earth-Science Reviews*, v. 136, p. 301–338.
- POWELL, M., OCKELFORD, A., RICE, S., HILLIER, J., NGUYEN, T., REID, I., TATE, N., AND ACKERLEY, D., 2016, Structural properties of mobile armors formed at different flow strengths in gravel-bed rivers: *Journal of Geophysical Research*, *Earth Surface*, v. 121, p. 1491–1515.
- QIN, J., AND NG, S., 2012, Estimation of effective roughness for water-worked gravel surfaces: *Journal of Hydraulic Engineering*, v. 138, p. 923–934.
- RAVEN, E., LANE, S., FERGUSON, R., AND BRACKEN, L., 2009, The spatial and temporal patterns of aggradation in a temperate, upland, gravel-bed river: *Earth Surface Processes and Landforms*, v. 34, p. 1181–1197.
- RICE, S., AND CHURCH, M., 2010, Grain-size sorting within river bars in relation to downstream fining along a wandering channel: *Sedimentology*, v. 57, p. 232–251.
- RICE, S., CHURCH, M., WOOLDRIDGE, C., AND HICKIN, E., 2009, Morphology and evolution of bars in a wandering gravel-bed river: lower Fraser river, British Columbia, Canada: *Sedimentology*, v. 56, p. 709–736.
- RÜTHER, N., HUBER, S., SPILLER, S., AND ABERLE, J., 2013, Verifying a photogrammetric method to quantify grain size distribution of developed armor layers: International Association for Hydro-Environment Engineering and Research Congress, Beijing, Proceedings.
- SMART, G.M., DUNCAN, M.J., AND WALSH, J.M., 2002, Relatively rough flow resistance equations: *Journal of Hydraulic Engineering*, v. 128, p. 568–578.
- SMART, G., ABERLE, J., DUNCAN, M., AND WALSH, J., 2004, Measurement and analysis of alluvial bed roughness: *Journal of Hydraulic Research*, v. 42, p. 227–237.
- SMITH, M., 2014, Roughness in the Earth Sciences: *Earth-Science Reviews*, v. 136, p. 202–225.
- STÄHLY, S., FRIEDRICH, H., AND DETERT, M., 2017, Size ratio of fluvial grains' intermediate axes assessed by image processing and square-hole sieving: *Journal of Hydraulic Engineering*, v. 143, 06017005.
- STERNBERG, H., 1875, Untersuchungen über Längen und Querprofil geschiebeführender Flüsse: *Zeitschrift für Bauwesen*, v. 25, p. 483–506.
- TUUNDER, A.P., AND RIBBERINK, J.S., 2012, Experimental observation and modeling of roughness variation due to supply-limited sediment transport in uni-directional flow: *Journal of Hydraulic Research*, v. 50, p. 506–520.
- VÁZQUEZ-TARRIO, D., BORGNIET, L., LIÉBAULT, F., AND RECKING, A., 2017, Using UAS optical imagery and SfM photogrammetry to characterize the surface grain size of gravel bars in a braided river (Vénénon River, French Alps): *Geomorphology*, v. 285, p. 94–105.
- WILCOCK, P., 1996, Estimating local bed shear stress from velocity observations: *Water Resources Research*, v. 32, p. 3361–3366.